



# Photocatalytic reduction of CO<sub>2</sub> over exposed-crystal-face-controlled TiO<sub>2</sub> nanorod having a brookite phase with co-catalyst loading

Teruhisa Ohno<sup>a,b,c,\*</sup>, Takayoshi Higo<sup>a</sup>, Naoya Murakami<sup>a,c</sup>, Hirofumi Saito<sup>a</sup>, Qitao Zhang<sup>a</sup>, Yin Yang<sup>a</sup>, Toshiki Tsubota<sup>a</sup>

<sup>a</sup> Department of Materials Science, Faculty of Engineering, Kyushu Institute of Technology, 1-1 Sensuicho, Tobata, Kitakyushu 804-8550, Japan

<sup>b</sup> JST, PRESTO, 4-1-8 Honcho Kawaguchi, Saitama 332-0012, Japan

<sup>c</sup> JST, ACT-C, 4-1-8 Honcho Kawaguchi, Saitama 332-0012, Japan

## ARTICLE INFO

### Article history:

Received 1 November 2013

Received in revised form 22 January 2014

Accepted 26 January 2014

Available online 3 February 2014

### Keywords:

Exposed-crystal-face-controlled TiO<sub>2</sub>

Brookite TiO<sub>2</sub> nanorod

Separation of reaction sites

Reduction of carbon dioxide

## ABSTRACT

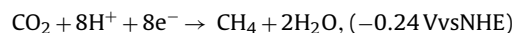
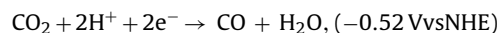
Photocatalytic reduction of carbon dioxide (CO<sub>2</sub>) was carried out using exposed-crystal-face-controlled titanium(IV) oxide (TiO<sub>2</sub>) having a brookite phase. Methanol (CH<sub>3</sub>OH) was detected as the main product, and trace amounts of formic acid, carbon monoxide, methane, and hydrogen were also detected in some cases. The prepared nanorod-shaped brookite TiO<sub>2</sub> with large {2 1 0} and small {2 1 2} exposed crystal faces showed larger CH<sub>3</sub>OH generation than that of commercial brookite TiO<sub>2</sub> powder (Kojundo Chemical Laboratory Co., Ltd.). The activity of a brookite TiO<sub>2</sub> nanorod for CO<sub>2</sub> reduction depended on its aspect ratio because the {2 1 0} crystal faced worked as a reduction site, whereas an oxidation site was assigned to {2 1 2} crystal faces. Photodeposition of gold (Au) or silver (Ag) nanoparticles on the nanorod-shaped brookite TiO<sub>2</sub> induced a dramatic increase in CH<sub>3</sub>OH production because the deposited metal particles work as reductive sites for multi-electron reduction of CO<sub>2</sub>. Among the co-catalyst-loaded brookite TiO<sub>2</sub> nanorods, nanorod-shaped brookite TiO<sub>2</sub> loaded with Ag showed higher activity. The source of carbon of CH<sub>3</sub>OH obtained by CO<sub>2</sub> reduction is discussed on the basis of results of a labeling experiment using <sup>13</sup>CO<sub>2</sub>.

© 2014 Elsevier B.V. All rights reserved.

## 1. Introduction

Practical application of photocatalysts in converting solar light to chemical energy has been an attractive research field [1–11]. Water splitting over photoirradiated semiconductor photocatalysts has become an important issue world wide [12–20] because hydrogen is a promising alternative fuel when fossil fuels become depleted. In addition, CO<sub>2</sub> reduction to produce usable products is an important topic from the viewpoint of not only an environmental issue but also artificial photosynthesis. Although reduction of CO<sub>2</sub> using semiconductors such as TiO<sub>2</sub> as a photocatalyst was reported by Fujishima [21], progress in this field has been very slow compared to the progress made in development of water splitting for hydrogen evolution. Photocatalytic reaction using semiconductor photocatalysts has been reported to have the potential to reduce CO<sub>2</sub> into hydrocarbons using water as an electron donor. For example, oxide semiconductor photocatalysts including titanium(IV) oxide (TiO<sub>2</sub>) can produce formic acid (HCOOH), formaldehyde (HCHO), methanol (CH<sub>3</sub>OH), and methane (CH<sub>4</sub>) [22–34]. However, quantum yields for photocatalytic CO<sub>2</sub> reduction have

been low. One reason for the low yields is that most of the reactions for CO<sub>2</sub> reduction employ a multi-electron process with relatively high redox potential, as shown below. In addition, back reaction on the surface of a semiconductor photocatalyst easily proceeded, resulting in retardation of CO<sub>2</sub> reduction, because many kinds of intermediates would be involved in this multi-electron reaction.



Therefore, control of reaction sites on the surfaces of photocatalysts is a promising strategy for improvement of CO<sub>2</sub> reduction. In order to control reaction sites on the surface of a TiO<sub>2</sub> photocatalyst, we developed technology for controlling exposed crystal faces of TiO<sub>2</sub> nanoparticles [35–43]. The exposed crystal surfaces worked as reduction sites and oxidation sites separately, resulting in improvement of photocatalytic activity for organic pollutant decomposition. These surface properties should be useful for improvement of a multi-electron reaction such as CO<sub>2</sub> reduction

\* Corresponding author at: Kyushu Institute of Technology, Department of Materials Science, Faculty of Engineering, 1-1 Sensui-cho, Tobata-ku, Tobata, Kitakyushu 804-8550, Japan. Tel.: +81 93 884 3318; fax: +81 93 884 3318.

E-mail address: [tohno@che.kyutech.ac.jp](mailto:tohno@che.kyutech.ac.jp) (T. Ohno).

because back reactions on the surfaces of photocatalysts would be drastically retarded.

Kominami et al. prepared single-phase brookite  $\text{TiO}_2$  powder for the first time by solvothermal synthesis in which oxobis(2,4-pentanedionato- $O,O'$ )titanium was used as the  $\text{TiO}_2$  precursor and sodium laurate was used as a reagent for controlling the crystal structure [44]. They subsequently investigated the photocatalytic activity of single-phase brookite  $\text{TiO}_2$  [45,46]. Recently, other groups have also reported single-phase brookite  $\text{TiO}_2$  having several kinds of characteristic structures, e.g., nanorods and nanotubes [47–51]. Among the three kinds of crystal structure of  $\text{TiO}_2$ , brookite  $\text{TiO}_2$  shows the highest reduction ability from evaluation of conduction band potential [52]. These properties are advantageous for  $\text{CO}_2$  reduction. Therefore, we developed exposed-crystal-face-controlled brookite  $\text{TiO}_2$  for  $\text{CO}_2$  reduction.

In addition, metal co-catalyst loading on semiconductor photocatalysts is frequently carried out to enhance quantum yield and selectivity from  $\text{CO}_2$  reduction into these products because appropriate co-catalysts work as reduction sites and enhance multi-electron reduction as a result of capturing electrons on metal particles [31,32,34,22,24,53,26–28,30].

As mentioned above, we developed shape-controlled  $\text{TiO}_2$  with specific exposed crystal faces in order to improve photocatalytic efficiency [35–43]. Utilization of the shape-controlled  $\text{TiO}_2$  enhanced photocatalytic activity for decomposition of an organic compound because spatial separation of redox sites was induced by different kinds of exposed crystal faces [35–43]. Moreover, this property has advantages in co-catalyst loading by a photodeposition method, and site-selective co-catalyst loading on reduction faces by the photodeposition technique, which possibly decreases the recombination rate in co-catalyst particles, enhances photocatalytic activity by retarding back reactions. Actually, metal particles on reduction faces were observed in the shape-controlled  $\text{TiO}_2$  [35–43].

In the present study, we confirmed the advantage of photocatalytic  $\text{CO}_2$  reduction by exposed-crystal-face-controlled brookite  $\text{TiO}_2$ . Moreover, the effect of co-catalyst loading on the exposed-crystal-face-controlled brookite  $\text{TiO}_2$  on activity for photocatalytic reduction of  $\text{CO}_2$  was examined. Labeling experiments using  $^{13}\text{CO}_2$  were also carried out in order to elucidate the carbon source of  $\text{CH}_3\text{OH}$  as a main product for  $\text{CO}_2$  reduction on exposed-crystal-face-controlled brookite  $\text{TiO}_2$  with co-catalyst loading.

## 2. Experimental

### 2.1. Materials

A titanium precursor (titaniumethoxide) was purchased from Sigma-Aldrich. Hydrogen peroxide (30%), ammonia, glycolic acid, polyvinyl alcohol (PVA), and polyvinyl pyrrolidone (PVP) were purchased from Wako Pure Chemical Industries, Ltd. Glycolic acid was used to control the crystallinity and morphology of brookite  $\text{TiO}_2$  particles. Commercial brookite  $\text{TiO}_2$  powder was obtained from Kojundo Chemical Laboratory Co., Ltd. Other chemical reagents used in the present study were commercial products without further treatment.

### 2.2. Procedure for preparation of brookite $\text{TiO}_2$ nanorods without a polymer

Morphology-controlled brookite  $\text{TiO}_2$  with  $\{210\}$  and  $\{212\}$  exposed crystal faces was prepared by hydrothermal synthesis [52,55–57].

The procedure for preparation of morphology-controlled  $\text{TiO}_2$  without an aspect ratio control reagent such as PVA is as follows.

Milli-Q water ( $3.0\text{ cm}^3$ ) was added to  $10\text{ cm}^3$  of titanium(IV) ethoxide and  $50\text{ cm}^3$  of ethanol with vigorous stirring, and the mixture was stirred for 30 min at room temperature. The resulting precipitate was centrifugally separated from the solution and dried under reduced pressure. The obtained amorphous titanium hydroxide particles ( $12.5\text{ mmol}$ ) were dispersed in 30% hydrogen peroxide ( $40.0\text{ cm}^3$ ). Then 25% ammonia ( $10.0\text{ cm}^3$ ) and glycolic acid ( $18.75\text{ mmol}$ ) were added, and yellow peroxo titanate acid (PTA) solution was obtained. After stirring the solution at ca.  $60^\circ\text{C}$  for 6 h to remove excess amounts of hydrogen peroxide and ammonia, an orange gelled compound was obtained. The gelled compound was dispersed in Milli-Q water ( $3.0\text{ cm}^3$ ) and pH of the solution was adjusted to 10 by addition of ammonia. Then the volume of the solution was adjusted ( $50.0\text{ cm}^3$ ) by addition of Milli-Q water, and the solution in a Teflon bottle sealed with a stainless jacket (Sanaikagaku Co., HU-100) was heated at  $200^\circ\text{C}$  for 48 h in an oven. After hydrothermal treatment, the residue in the Teflon bottle was washed with Milli-Q water until ionic conductivity of the supernatant was  $<10\text{ }\mu\text{S cm}^{-1}$ . The particles were dried under reduced pressure at  $60^\circ\text{C}$  for 12 h.

### 2.3. Procedure for preparation of brookite $\text{TiO}_2$ nanorods with a polymer as an aspect ratio control reagent

Milli-Q water ( $3.0\text{ cm}^3$ ) was added to  $10\text{ cm}^3$  of titanium(IV) ethoxide and  $50\text{ cm}^3$  of ethanol with vigorous stirring, and the mixture was stirred for 30 min at room temperature. The resulting precipitate was centrifugally separated from the solution and dried under reduced pressure. The obtained amorphous titanium hydroxide particles ( $25.0\text{ mmol}$ ) were dispersed in 30% hydrogen peroxide ( $40.0\text{ cm}^3$ ). Then 25% ammonia ( $10.0\text{ cm}^3$ ) and glycolic acid ( $50.0\text{ mmol}$ ) were added, and yellow peroxo titanate acid (PTA) solution was obtained. An aqueous solution containing an appropriate amount of PVA or PVP was added to the PTA solution. After stirring the solution at room temperature for 6 h to remove excess amounts of hydrogen peroxide and ammonia, an orange gelled compound was obtained. The gelled compound was dispersed in Milli-Q water ( $3.0\text{ cm}^3$ ) and pH of the solution was adjusted to 10 by addition of ammonia. Then the volume of the solution was adjusted ( $50.0\text{ cm}^3$ ) by addition of Milli-Q water, and the solution in a Teflon bottle sealed with a stainless jacket (Sanaikagaku Co., HU-100) was heated at  $200^\circ\text{C}$  for 48 h in an oven. After hydrothermal treatment, the residue in the Teflon bottle was washed with Milli-Q water until ionic conductivity of the supernatant was  $<10\text{ }\mu\text{S cm}^{-1}$ . The particles were dried under reduced pressure at  $60^\circ\text{C}$  for 12 h.

### 2.4. Photodeposition of Au or Ag co-catalyst on brookite $\text{TiO}_2$ particles

For photodeposition of Au, an aqueous suspension consisting of brookite  $\text{TiO}_2$  particles ( $200\text{ mg}$ ) and  $50\text{ mL}$  of an ethanol solution (8 vol%) containing an appropriate amount of hydrogen tetrachloroaurate(III) tetrahydrate was photoirradiated with a light-emitting diode (Nichia, NCCU033), which emitted light at a wavelength of ca.  $365\text{ nm}$  and an intensity of  $0.3\text{ mW cm}^{-2}$ , under a nitrogen atmosphere with vigorous magnetic stirring for 24 h. For photodeposition of Ag, an aqueous suspension consisting of  $\text{TiO}_2$  particles ( $200\text{ mg}$ ) and  $50\text{ mL}$  of Milli-Q water containing an appropriate amount of silver nitrate was photoirradiated under the same conditions. After irradiation, photodeposited samples were obtained by washing with water several times and drying. The net amount of Au or Ag on the  $\text{TiO}_2$  surface was estimated by analysis of the filtrate with inductively coupled plasma optical emission spectroscopy (ICPOES; Shimadzu, ICPS-8000). ICP analysis revealed that the net molar amounts of Au and Ag compounds photodeposited

on the brookite  $\text{TiO}_2$  by photodeposition were more than 99% of the provided molar amounts of Au and Ag.

### 2.5. Characterization of prepared samples

Crystal structures of the  $\text{TiO}_2$  powders were characterized by using an X-ray diffractometer (Rigaku, MiniFlex II) with  $\text{Cu K}\alpha$  radiation ( $\lambda = 1.5405 \text{ \AA}$ ). Primary particle sizes of the prepared samples were estimated from peaks at  $37^\circ$  which are attributed to brookite  $\{1\ 2\ 1\}$  in XRD patterns using the Scherrer equation:  $d = 0.9\lambda / \beta \cos\theta$ , where  $\lambda$  is the wavelength of X-rays,  $\theta$  is the Bragg angle and  $\beta$  is the full width at half maximum.  $\beta$  was estimated by fitting the XRD patterns with a superposition of Lorentz functions for peaks attributed to brookite. Diffuse reflectance (DR) spectra were measured using a UV–VIS spectrometer (Shimadzu, UV-2500PC and 2600) equipped with an integrating sphere unit (ISR-240A and ISR-2600plus). Specific surface area ( $S_{\text{BET}}$ ) of the particles was determined with a surface area analyzer (Quantachrome, Nova 4200e) by using the Brunauer–Emmett–Teller equation. The morphology of prepared  $\text{TiO}_2$  particles was observed by using a scanning electron microscope (SEM; JEOL, JSM-6701FONO) and a transmission electron microscope (TEM; Hitachi, H-9000NAR). X-ray photoelectron spectroscopy (XPS) spectra were obtained by using Kratos AXIS NOVA equipped with an Al  $\text{K}\alpha$  X-ray source of the dual anode. The shift of binding energy was corrected using the C 1s level at 284.6 eV as an internal standard. The net amounts of Au or Ag compounds on the hybrid photocatalysts were estimated by analysis of the filtrate with inductively coupled plasma optical emission spectroscopy (ICP-OES; Shimadzu, ICPS-8000).

### 2.6. Photocatalytic reduction of $\text{CO}_2$

Before evaluation of the photocatalytic activity, each sample was irradiated with UV light using black light (UVP, XX-15BLB) for one day in order to remove organic compounds on the sample.  $^1\text{O}_2$  (15 mM) treatment of the photocatalysts was performed for 2 h by using  $^1\text{O}_2$  generator (EKBIO-1100, Ebara Jitsugyo Co. Ltd) just before photocatalytic reduction of  $\text{CO}_2$  experiments. Photocatalytic reduction of  $\text{CO}_2$  was carried out under ambient pressure. A light-emitting diode (Nichia, NCCU033), which emitted light at a wavelength of ca. 365 nm and an intensity of  $0.3 \text{ mW cm}^{-2}$ , was used as the light source for photocatalytic evaluation, and a test tube containing 5 mg of  $\text{TiO}_2$  and 5 mL of  $0.2 \text{ mol L}^{-1} \text{ KHCO}_3$  aqueous solution saturated with  $\text{CO}_2$  was photoirradiated with stirring for 24 h. Reaction products in liquid and gas phases were analyzed by gas chromatography (Hitachi G-3500, FID detector) with DB-WAXETR columns, gas chromatography (GL Science 490-GC, micro TCD detector) with MS-5A columns, and ion chromatography (Dionex, ICS-900) with IonPac AS-12A columns. Spherical shaped brookite  $\text{TiO}_2$  was used as commercial brookite  $\text{TiO}_2$  powder.

Apparent quantum efficiency (QE) was defined by the following equation because of a 6-hole process for production of  $\text{CH}_3\text{OH}$  as a main product from  $\text{CO}_2$  reduction.

$$\begin{aligned} \text{QE} &= \frac{\text{Number of reacted electrons}}{\text{Number of incident photons}} \\ &= \frac{\text{Number of generated } \text{CH}_3\text{OH molecules} \times 6}{\text{Number of incident photons}} \times 100 \end{aligned}$$

### 2.7. Reactivity evaluation of exposed crystal faces by photodeposition of Pt and lead(IV) oxide ( $\text{PbO}_2$ ) on brookite $\text{TiO}_2$ nanorods

Photodeposition of Pt and  $\text{PbO}_2$  were carried out to determine reduction and oxidation sites on  $\text{TiO}_2$  particles, respectively

[58]. For determination of reduction sites, exposed crystal surface photodeposition of Pt was performed. An aqueous brookite  $\text{TiO}_2$  nanorod suspension ( $2 \text{ g L}^{-1}$ ) containing  $0.52 \text{ M}$  2-propanol and  $1 \text{ mM}$  hexachloroplatinic acid ( $\text{H}_2\text{PtCl}_6 \cdot 6\text{H}_2\text{O}$ ) was irradiated with a 300 W mercury UV lamp (WACOM Model XDS-501S) for 24 h.  $\text{N}_2$  gas was vigorously purged through the suspension prior to UV irradiation. The light intensity was about  $1 \text{ mW cm}^{-2}$ . After irradiation, the color of the powder changed from white to silver, and the suspension was centrifuged and washed with distilled water and then collected as powder after drying for 5 h at  $60^\circ\text{C}$  under reduced pressure.

$\text{PbO}_2$  nanoparticles were deposited as a result of  $\text{Pb}^{2+}$  ion oxidation in order to identify oxidation sites on the surface of brookite  $\text{TiO}_2$  nanorods. This reaction was carried out in an aqueous brookite  $\text{TiO}_2$  nanorod suspension ( $2 \text{ g L}^{-1}$ ) containing  $0.1 \text{ M}$   $\text{Pb}(\text{NO}_3)_2$  under an aerated condition. The pH of the solution for this reaction was adjusted to 1.0 by the addition of nitric acid according to the literature [58]. After photoreaction for 24 h using a 500 W Hg lamp (USHIO Co. Ltd., SX-UI501HQ), the color of the powder changed from white to brown, indicating that  $\text{PbO}_2$  had been deposited on the surface. The light intensity was about  $0.1 \text{ W cm}^{-2}$ . Pt and  $\text{PbO}_2$  particles deposited on  $\text{TiO}_2$  were observed in SEM, EDX and TEM images.

## 3. Results and discussion

### 3.1. Characterization

Fig. 1 shows an XRD pattern of the prepared  $\text{TiO}_2$ . The structure of prepared sample was attributed to single-phase brookite  $\text{TiO}_2$ . Fig. 2 shows a TEM image of the prepared  $\text{TiO}_2$ . Rod-like morphology with a length of 115 nm and width of 35 nm, which were agreed with the primary particle size estimated from the XRD pattern. Assignment of these exposed crystal faces was confirmed by SEM (Fig. 3), TEM (Fig. 2) and selected area electron diffraction (SAED) analyses. The prepared  $\text{TiO}_2$  showed a nanorod shape with large  $\{2\ 1\ 2\}$  and small  $\{2\ 1\ 0\}$  exposed crystal faces, indicating that the nanorod-shaped particles were single crystals.  $S_{\text{BET}}$  of the prepared  $\text{TiO}_2$  was  $45 \text{ m}^2 \text{ g}^{-1}$ .

### 3.2. Effect of PVA or PVP as an aspect ratio control reagent ( $T=48 \text{ h}$ , $\text{pH } 7$ )

To determine the role of PVA or PVP in the reaction, we conducted a series of syntheses by varying the concentration of PVA or PVP. TEM and SEM images showed that addition of the PVA or PVP

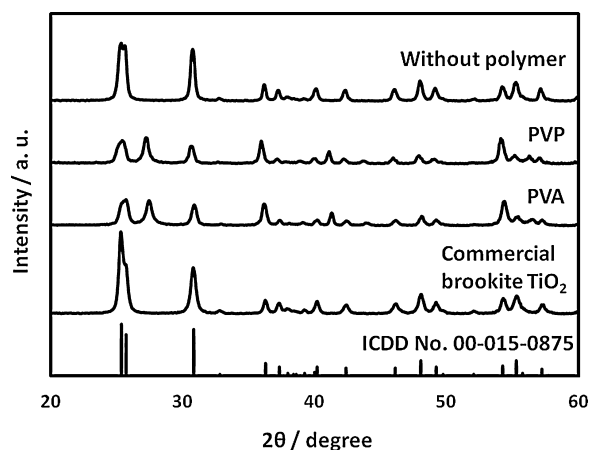


Fig. 1. XRD pattern.



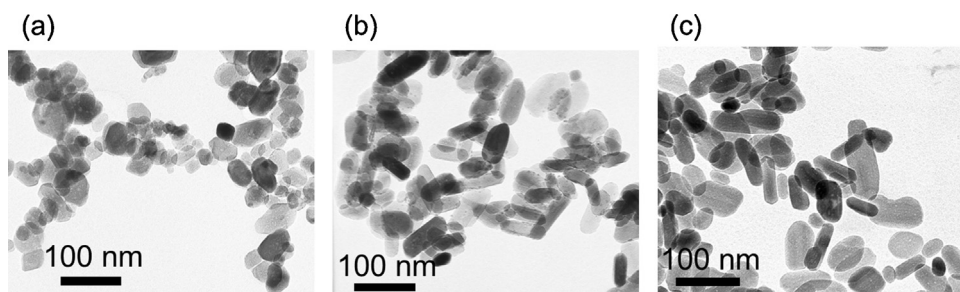


Fig. 2. TEM images of brookite  $\text{TiO}_2$  nanorod (a) with PVA (b) with PVP and (c) without polymer.

polymer resulted in control of the shape of  $\text{TiO}_2$  nanorods. Fig. 2(a and b) shows TEM images of brookite  $\text{TiO}_2$  nanorods obtained after hydrothermal treatment with different PVA or PVP concentrations. TEM images without a polymer (Fig. 2(c)) showed a rod-like shape with an aspect ratio of 2.7 and single crystalline quality of the brookite  $\text{TiO}_2$  nanorod.

The aspect ratio of brookite  $\text{TiO}_2$  nanorods was decreased by addition of PVA or PVP. The effect of aspect ratio control for a brookite  $\text{TiO}_2$  nanorod by addition of PVA was greater than that by addition of PVP as shown in Fig. 2(a–b). These results indicate that addition of 50 mg of PVA was sufficient to prepare brookite  $\text{TiO}_2$  particles with a small aspect ratio (Fig. S1). The aspect ratio of a brookite  $\text{TiO}_2$  nanorod with specific exposed crystal faces is sensitive to photocatalytic activity for  $\text{CO}_2$  reduction, as discussed in a later section. The ratio of exposed reduction sites to oxidation sites on the surface of a brookite  $\text{TiO}_2$  nanorod should be controlled in order to improve  $\text{CO}_2$  reduction. Under the optimized conditions, reduction sites on the surface of a brookite  $\text{TiO}_2$  nanorod should be predominantly exposed.

### 3.3. Photodeposition of Pt and $\text{PbO}_2$ for determination of reduction and oxidation sites

In order to determine reactivity such as oxidation or reduction on the exposed crystal surface of brookite  $\text{TiO}_2$ , photodeposition of Pt and  $\text{PbO}_2$  was carried out. The colors of  $\text{TiO}_2$  powder after UV irradiation in the presence of  $\text{H}_2\text{PtCl}_6$  and  $\text{Pb}(\text{NO}_3)_2$  aqueous solutions changed to gray and brown, respectively [58]. These color change in brookite  $\text{TiO}_2$  suggested that Pt and  $\text{PbO}_2$  were deposited on the  $\text{TiO}_2$  surface. Furthermore, the presence of Pt and Pb elements was confirmed by XPS analysis. Pt particles were efficiently deposited on the exposed crystal surface assigned to reduction site because of  $\text{Pt}^{4+}$  reduction. The oxidation site of exposed crystal surface was assigned to  $\text{PbO}_2$  deposition because  $\text{Pb}^{4+}$  was oxidized to produce  $\text{PbO}_2$  nanoparticles. Fig. 4 shows TEM images of Pt- and  $\text{PbO}_2$ -deposited brookite  $\text{TiO}_2$  nanorods that were prepared by 48 h of hydrothermal treatment with PTA solution containing glycolic acid without a polymer. Small particles were observed on the

specific exposed face of the brookite  $\text{TiO}_2$  nanorod. Small particles were assigned by TEM with EDX analysis to Pt or  $\text{PbO}_2$  deposited on the reductive or oxidative crystal surface of the brookite  $\text{TiO}_2$  nanorod (Fig. 4). Pt nanoparticles of ca. 10 nm in size were mainly observed on the  $\{210\}$  face of a brookite  $\text{TiO}_2$  nanorod, while large  $\text{PbO}_2$  particles with sizes of more than 100 nm were deposited on the  $\{212\}$  face of a brookite  $\text{TiO}_2$  nanorod. These smaller particles were not observed on  $\text{TiO}_2$  particles before the photodeposition procedure (Fig. 4).

As described in a later section, a correlation was found between photocatalytic activity and surface structure of  $\text{TiO}_2$  particles, and photocatalytic activity increased with increase in the aspect ratio of brookite  $\text{TiO}_2$  nanorods, which indicate the ratio of  $\{210\}$  to  $\{212\}$  exposed crystal faces. This result suggests that brookite  $\text{TiO}_2$  nanorods with a small surface area of  $\{212\}$  and large surface area of  $\{210\}$  are suitable for photocatalytic  $\text{CO}_2$  reduction. The highest photocatalytic activity of a brookite  $\text{TiO}_2$  nanorod prepared by 48 h of hydrothermal treatment in the absence of a polymer was mainly due to the larger surface areas of reduction sites on the nanorod  $\text{TiO}_2$  structure with the largest aspect ratio.

### 3.4. Photocatalytic activity for $\text{CO}_2$ reduction over a brookite $\text{TiO}_2$ nanorod with exposed crystal surfaces

In this study, amounts of the gas phase products are a trace (under the detection limit of Gas chromatography) over photoirradiation of co-catalyst loaded brookite  $\text{TiO}_2$ . When bare brookite  $\text{TiO}_2$  was used, amounts of  $\text{H}_2$ ,  $\text{CO}$ ,  $\text{CH}_4$  products are about 8, 3, 0 nmol, respectively. And amount of  $\text{HCOOH}$  is 35 nmol under ionic chromatography. Eventually,  $\text{CH}_3\text{OH}$  is a main product for the  $\text{CO}_2$  reduction by using prepared brookite  $\text{TiO}_2$  photocatalysts without co-catalyst. Photocatalytic reductions of  $\text{CO}_2$  in our systems were performed in an aqueous suspension of prepared brookite  $\text{TiO}_2$  at pH 7.3. Under the condition, the ionic forms of  $\text{CO}_2$  in aqueous media should be a mixture of  $\text{HCO}_3^-$ ,  $\text{H}_2\text{CO}_3$ . Redox potentials of  $\text{CO}_3^{2-}$ ,  $\text{H}_2\text{CO}_3$  are +0.209, +0.044 V vs NHE for methanol formation from  $\text{CO}_2$  reduction, respectively [59]. In addition, redox potentials of  $\text{HCO}_3^-$  might be placed between +0.209 and +0.044 V

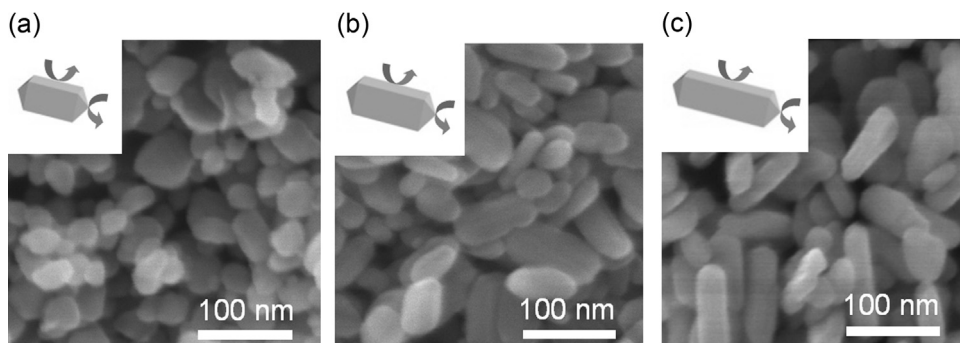


Fig. 3. SEM images of the prepared brookite  $\text{TiO}_2$  nanorod (a) with PVA (b) with PVP and (c) without polymer.

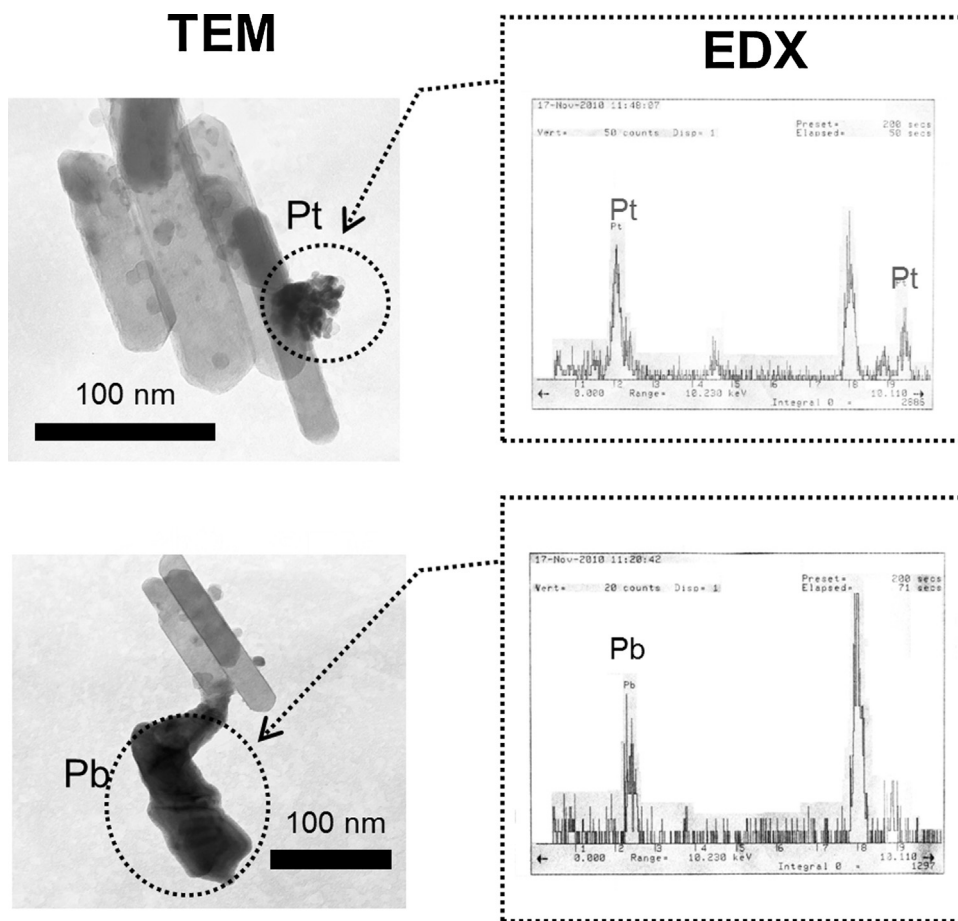


Fig. 4. TEM images and EDX analyses of Pt or PbO<sub>2</sub> loaded brookite TiO<sub>2</sub> nanorods (a) Pt (b) PbO<sub>2</sub>.

vs NHE. Fig. 5 shows CH<sub>3</sub>OH generation for the prepared brookite TiO<sub>2</sub> nanorod and commercial brookite TiO<sub>2</sub>, which are non shape-controlled particles with  $S_{\text{BET}}$  of 27 m<sup>2</sup> g<sup>−1</sup>. CH<sub>3</sub>OH production by the prepared brookite TiO<sub>2</sub> nanorod was 2-times greater than that by spherical shaped commercial brookite TiO<sub>2</sub>. This result indicated that a shape-controlled brookite TiO<sub>2</sub> nanorod with exposed crystal phases has higher activity for CO<sub>2</sub> reduction than non shape-controlled commercial brookite TiO<sub>2</sub>, presumably due to separation of oxidation and reduction sites. Moreover, larger {2 1 0} and smaller {2 1 2} exposed crystal faces may be an ideal surface structure for a multi-electron process for CO<sub>2</sub> reduction.

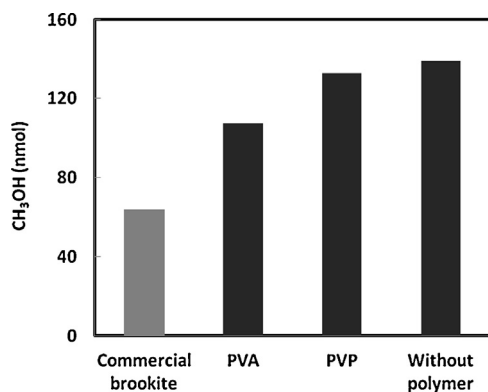


Fig. 5. Amount of CH<sub>3</sub>OH generated over several kinds of brookite TiO<sub>2</sub> (commercial brookite TiO<sub>2</sub>, the prepared brookite TiO<sub>2</sub> with PVA, PVP and without polymer).

As described above, the aspect ratio of a brookite nanorod was decreased by addition of PVA or PVP as an aspect control reagent to the reaction solution during hydrothermal treatment. Aspect ratio dependence of the photocatalytic activity of a brookite TiO<sub>2</sub> nanorod with exposed crystal surfaces for CO<sub>2</sub> reduction was observed. The photocatalytic activity of a brookite TiO<sub>2</sub> nanorod for CO<sub>2</sub> reduction was decreased when the aspect ratio of the brookite TiO<sub>2</sub> nanorod became lower by using PVA or PVP as an aspect ratio control reagent. Enlargement of {2 1 0} assigned to reduction sites is an important strategy for improvement of photocatalytic CO<sub>2</sub> reduction over a brookite TiO<sub>2</sub> nanorod under UV light.

### 3.5. Effect of co-catalyst loading on photocatalytic activity

For further improvement of photocatalytic activity for CO<sub>2</sub> reduction, Au or Ag particles as co-catalysts were loaded on the prepared brookite TiO<sub>2</sub> nanorod by the photodeposition method. It was expected that the co-catalysts would be deposited on {2 1 0} exposed crystal faces of the prepared brookite TiO<sub>2</sub> nanorod because reduction reaction ( $\text{Au}^{3+} + 3\text{e}^- \rightarrow \text{Au}^0$ ,  $\text{Ag}^+ + \text{e}^- \rightarrow \text{Ag}^0$ ) predominantly proceeds over {2 1 0} faces of a brookite TiO<sub>2</sub> nanorod. Actually, loaded co-catalyst particles were observed mainly on {2 1 0} exposed crystal faces of the samples with larger amounts of Au and Ag loading as shown in Fig. 6.

After photodeposition, the color of the samples changed depending on the kind of loading material and loading amount. The colors of Au-loaded and Ag-loaded samples immediately after photodeposition were dark purple and pale henna, respectively. The colors of the samples correspond to localized surface plasmon resonance (LSPR) absorption of Au and Ag [60–63], and this

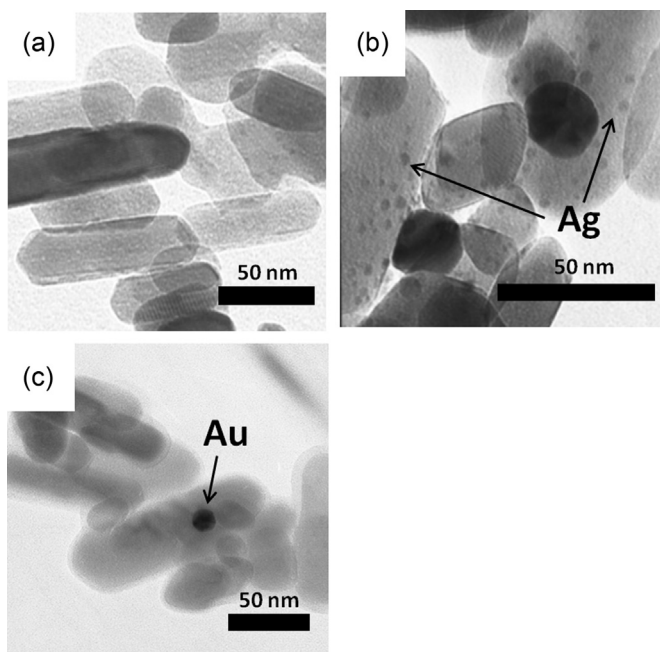


**Fig. 6.** TEM images of brookite  $\text{TiO}_2$  nanorods (a) bare sample and (b) Au loaded brookite  $\text{TiO}_2$  and (c) Ag loaded brookite  $\text{TiO}_2$ .

implies that some of the Au and Ag particles were present as a metal state. However, the color of Ag-loaded samples changed after pre-treatment for photocatalytic activity (UV irradiation for removal of organic compounds on the sample), indicating that aggregation of Ag nanoparticles or oxidation of Ag to generate  $\text{Ag}_2\text{O}$  might have occurred [34]. Fig. 7 shows DR spectra of the prepared

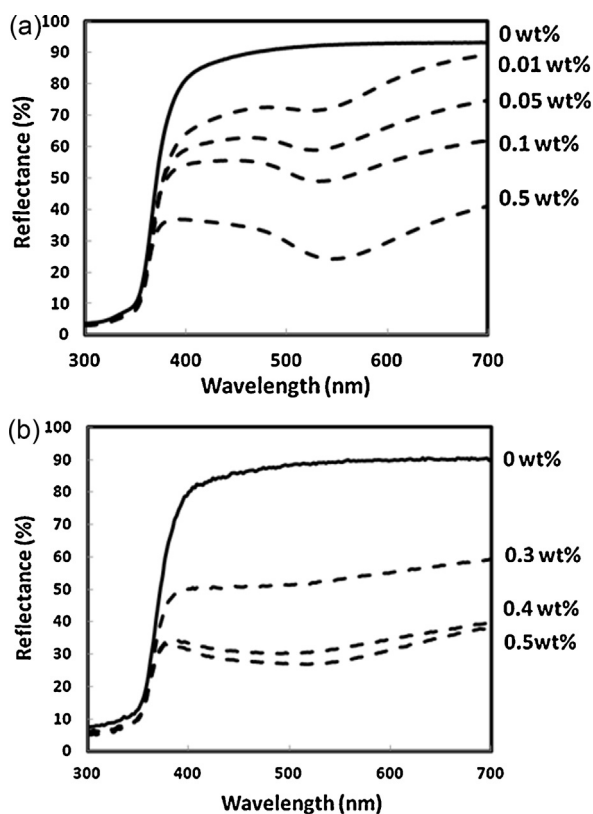


**Fig. 7.** DR spectra of metal co-catalysts loaded brookite  $\text{TiO}_2$  nanorods (a) Au and (b) Ag.

brookite  $\text{TiO}_2$  nanorod with Au or Ag loading just before photocatalytic evaluation. Absorption peaks around 550 nm and 500 nm, which correspond to LSPR of Au and Ag on  $\text{TiO}_2$ , were observed in Au-loaded and Ag-loaded  $\text{TiO}_2$  samples, respectively [60–62]. This implies that some of the Au and Ag particles were presumably present as a metal state after the pre-treatment for photocatalytic activity. Actually, XPS measurements were carried out on the Au-loaded and Ag-loaded  $\text{TiO}_2$  samples (Fig. S2). XPS spectra showed that loaded Ag particles were present as a mixture of Ag and  $\text{Ag}_2\text{O}$ . In contrast, the XPS spectrum confirmed that loaded Au particles were present as metal without other oxidation states. This coincides with the unchanged color of Au-loaded samples after the pre-treatment for photocatalytic activity.

Fig. 8 shows  $\text{CH}_3\text{OH}$  generation of the prepared brookite  $\text{TiO}_2$  nanorod with Au or Ag loading.  $\text{CH}_3\text{OH}$  generation showed an optimum amount with co-catalyst loading in all cases. In photocatalytic reaction systems,  $\text{CO}_2$  reduction usually competes with  $\text{H}_2$  evolution as a result of  $\text{H}^+$  reduction. For instance,  $\text{H}_2$  evolution predominantly occurs over Pt-loaded  $\text{TiO}_2$  particles. On the other hand, Ag loading on the surface of a brookite  $\text{TiO}_2$  nanorod induces predominant  $\text{CO}_2$  reduction. Therefore, loading an optimum amount of a co-catalyst on the surface of brookite  $\text{TiO}_2$  improves the selectivity between  $\text{CO}_2$  reduction and  $\text{H}_2$  evolution as well as the photocatalytic activity for  $\text{CO}_2$  reduction. Although the key mechanism for highly selective  $\text{CO}_2$  reduction on co-catalyst-loaded brookite  $\text{TiO}_2$  is under investigation, preferential  $\text{CO}_2$  adsorption on a co-catalyst loaded on the surface of  $\text{TiO}_2$  particles might be one of the key steps for improving predominant  $\text{CO}_2$  reduction.

Increase in  $\text{CH}_3\text{OH}$  generation on brookite  $\text{TiO}_2$  loaded with a co-catalyst was presumably due to prevention of recombination and/or enhancement of selectivity for  $\text{CH}_3\text{OH}$  generation as a result of multi-electron reduction by electron capturing on metal

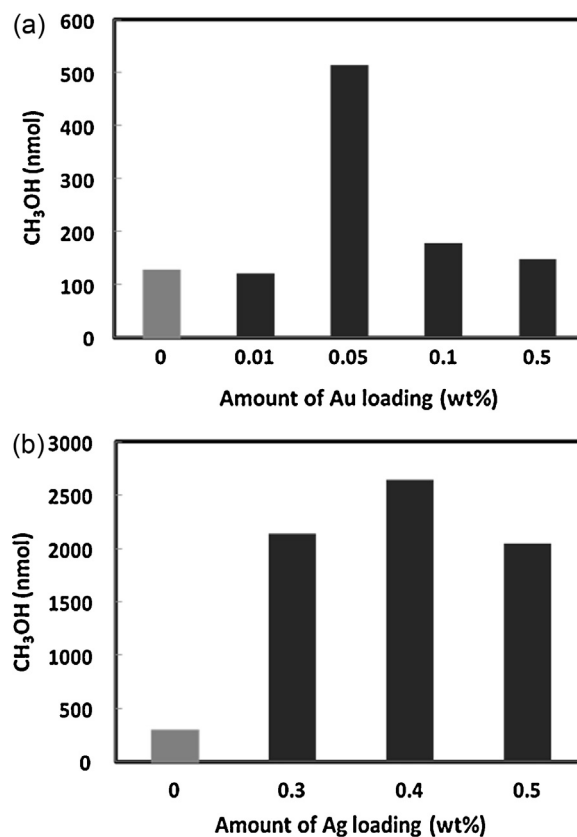


**Fig. 8.** Amount of  $\text{CH}_3\text{OH}$  generated over the metal co-catalysts loaded brookite  $\text{TiO}_2$  nanorods as a function of amount of co-catalysts (a) Au (b) Ag.

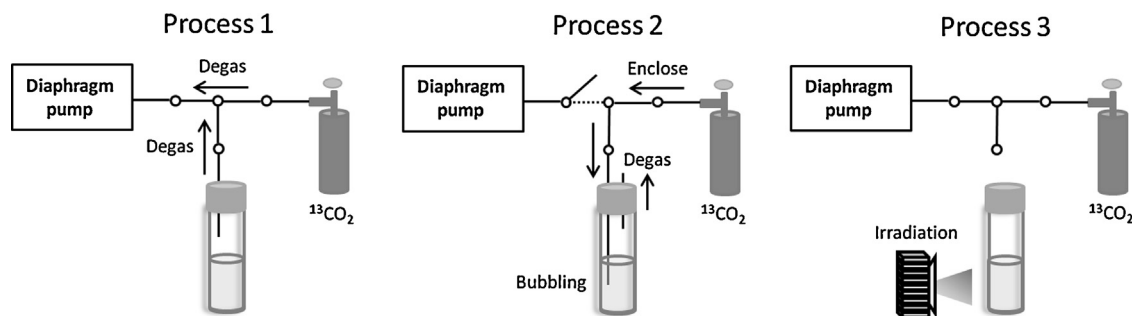


Fig. 9. Process of experiments reduction of CO<sub>2</sub> using <sup>13</sup>CO<sub>2</sub>.

particles. This effect was probably influenced by properties of co-catalyst particles, e.g., loading site, amount, particle size and dispersibility. Decrease in CH<sub>3</sub>OH generation with an excess amount of the co-catalyst may be due to the filter effect caused by photoabsorption and/or light scattering of co-catalyst particles. Actually, relative reflectance of the samples in the wavelength of more than 400 nm increased with an increase in loading amount (Fig. 8). Moreover, excess amount of co-catalyst loading may result in covering active sites or absorption sites of reactants and loss of appropriate properties as co-catalyst particles, such as dispersibility and particle size.

In order to elucidate the influence of particle size on CH<sub>3</sub>OH generation, absorption peaks attributed to LSPR of Au and Ag particles were evaluated in UV–VIS spectra (Fig. 8). Fig. 8 shows absorption wavelength of the peak ( $\lambda_p$ ) attributed to LSPR of Au and Ag as a function of amount of co-catalyst loading. A red shift of LSPR peak was usually observed by particle size growing and aggregation state of metal particles [63–65].

The peaks of Au-loaded samples showed dependence on loading amount up to 0.1 wt%. This indicates that the decrease in CH<sub>3</sub>OH generation by the 0.1 wt% Au-loaded sample was mainly caused by an increase in particle size and decrease in dispersion of Au particles. In contrast, the peaks of Ag-loaded samples were only slightly red-shifted with an increase in loading amount. This indicates that decrease in CH<sub>3</sub>OH generation with a larger amount of Ag loading might be due to the filter effect.

Therefore, CH<sub>3</sub>OH generation of the Au-loaded brookite TiO<sub>2</sub> nanorod was influenced by particle size and/or aggregation state in addition to the effect observed in the Ag-loaded sample.

### 3.6. Labeling experiments using <sup>13</sup>CO<sub>2</sub> reduction of CO<sub>2</sub>

We applied <sup>1</sup>H-NMR spectroscopy for analyzing the carbon source of CH<sub>3</sub>OH. Labeling experiment by using <sup>13</sup>CO<sub>2</sub> for CO<sub>2</sub> reduction was taken place over Au loaded brookite TiO<sub>2</sub> nanorod for 24 h under UV light irradiation. Before evaluation of the photocatalytic activity, each sample was irradiated with UV light using black light (UVP, XX-15BLB) for one day in order to remove organic compounds on the sample. <sup>1</sup>O<sub>2</sub> (15 mM) treatment of the photocatalysts was performed for 2 h by using <sup>1</sup>O<sub>2</sub> generator (EKBIO-1100, Ebara Jitsugyo Co. Ltd) just before photocatalytic reduction of CO<sub>2</sub> experiments. Degas and purge <sup>13</sup>CO<sub>2</sub> processes were shown in Fig. 9. Photocatalysts powder 5 mg were ultrasonically dispersed in deionized water (5 mL). After complete degassing the whole system by diaphragm pump (Process 1), <sup>13</sup>CO<sub>2</sub> gas was bubbling for 15 min (Process 2). CO<sub>2</sub> photoreduction is performed for 24 h during UV irradiation (Process 3). After the reaction, the photocatalysts was removed by centrifugal separation. The aqueous samples (4 mL) for <sup>1</sup>H-NMR are dissolved in D<sub>2</sub>O (1 mL). 3-(Trimethylsilyl)-1-propanesulfonic acid sodium salt (SIGMA-ALDRICH) was used as an internal standard compound. In the <sup>1</sup>H-NMR of the same solution,

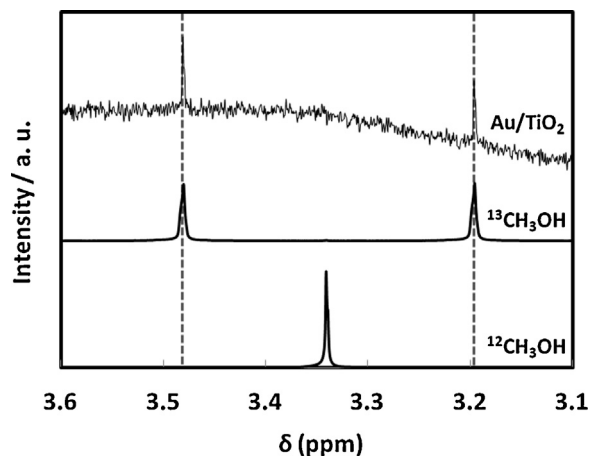


Fig. 10. <sup>1</sup>H-NMR spectra of Au-loaded brookite TiO<sub>2</sub> nanorod.

a doublet ( $J_{CH} = 142$  Hz) attributable to the proton coupled to the <sup>13</sup>C of <sup>13</sup>CH<sub>3</sub>O<sup>−</sup> was observed at 3.34 ppm, but no singlet due to the proton of <sup>12</sup>CH<sub>3</sub>O<sup>−</sup> was detected (Fig. 10). These results clearly show that the carbon source of CH<sub>3</sub>OH is <sup>13</sup>CO<sub>2</sub>.

## 4. Conclusion

Brookite TiO<sub>2</sub> particles with specific exposed crystal faces were prepared by hydrothermal treatment. In addition, PVP or PVA was used as an aspect control reagent. The aspect ratio of the prepared brookite TiO<sub>2</sub> nanorod was controlled by addition of PVA or PVP.

Photocatalytic CO<sub>2</sub> reduction using brookite TiO<sub>2</sub> nanorods with large {2 1 0} and small {2 1 2} exposed crystal faces were carried out. CH<sub>3</sub>OH was obtained as the main product for CO<sub>2</sub> reduction over a brookite TiO<sub>2</sub> nanorod under UV light. Photocatalytic activity of a brookite TiO<sub>2</sub> nanorod for CO<sub>2</sub> reduction is higher than that of spherical-shaped commercial brookite TiO<sub>2</sub>. In addition, a brookite TiO<sub>2</sub> nanorod with larger aspect ratio showed higher photocatalytic activity than that with a smaller aspect ratio. This indicates that larger {2 1 0} and smaller {2 1 2} exposed crystal faces prevented back reaction and enhanced multi-electron reduction as a result of separation of redox sites. Au or Ag loading on the reduction crystal surface of the prepared brookite TiO<sub>2</sub> nanorod increased CH<sub>3</sub>OH generation. The mechanisms of activity enhancement by the loading of metals might be different. Au loading increased selectivity for CH<sub>3</sub>OH generation to some extent. On the other hand, loading of Ag with appropriate properties resulted in a larger increase in CH<sub>3</sub>OH generation than that in the case of Au, though Ag has no selectivity for CH<sub>3</sub>OH generation. The carbon source of CH<sub>3</sub>OH, which is the main product of CO<sub>2</sub> reduction over a brookite TiO<sub>2</sub> nanorod, was confirmed by a labeling experiment using <sup>13</sup>CO<sub>2</sub>.



## Acknowledgments

This work was supported by the JST PRESTO program and the JST ACT-C program.

## Appendix A. Supplementary data

Supplementary data associated with this article can be found, in the online version, at <http://dx.doi.org/10.1016/j.apcatb.2014.01.048>.

## References

- [1] A. Fujishima, K. Honda, *Nature* 238 (1972) 37–38.
- [2] A. Fujishima, T.N. Rao, D.A. Tryk, *J. Photochem. Photobiol., C* 1 (2000) 1–21.
- [3] Y. Shiraishi, T. Hirai, *J. Photochem. Photobiol., C* 9 (2008) 157–170.
- [4] B. Ohtani, *J. Photochem. Photobiol., C* 11 (2010) 157–178.
- [5] T. Yui, Y. Kobayashi, Y. Yamada, K. Yano, Y. Fukushima, T. Torimoto, K. Takagi, *ACS Appl. Mater. Interfaces* 3 (2011) 931–935.
- [6] T. Yui, T. Tsuchino, H. Mino, T. Kajino, S. Itoh, Y. Fukushima, K. Takagi, *Bull. Chem. Soc. Jpn.* 82 (2009) 914–916.
- [7] T. Yui, Y. Kobayashi, Y. Yamada, T. Tsuchino, K. Yano, T. Kajino, Y. Fukushima, T. Torimoto, H. Inoue, K. Takagi, *Phys. Chem. Chem. Phys.* 8 (2006) 4585–4590.
- [8] T. Tachikawa, T. Yui, M. Fujitsuka, K. Takagi, T. Majima, *Chem. Lett.* 34 (2005) 1522–1523.
- [9] P.G. Hoertz, T.E. Mallouk, *Inorg. Chem.* 44 (2005) 6828–6840.
- [10] A.C. Benniston, A. Harriman, *Mater. Today* 11 (2008) 26–34.
- [11] T.E. Mallouk, *J. Phys. Chem. Lett.* 1 (2010) 2738–2739.
- [12] R. Abe, *J. Photochem. Photobiol., C* 11 (2010) 179–209.
- [13] M. Higashi, R. Abe, T. Takata, K. Domen, *Chem. Mater.* 21 (2009) 1543–1549.
- [14] K. Maeda, K. Teramura, D. Lu, T. Takata, N. Saito, Y. Inoue, K. Domen, *Nature* 440 (2006) 295.
- [15] I. Tsuji, Y. Shimodaira, H. Kato, H. Kobayashi, A. Kudo, *Chem. Mater.* 22 (2010) 1402–1409.
- [16] Y.K. Kho, A. Iwase, W.Y. Teoh, L. Madler, A. Kudo, R. Amal, *J. Phys. Chem. C* 114 (2010) 2821–2829.
- [17] H. Kaga, K. Saito, A. Kudo, *Chem. Commun.* 46 (2010) 3779–3781.
- [18] H. Kato, Y. Sasaki, A. Iwase, A. Kudo, *Bull. Chem. Soc. Jpn.* 80 (2007) 2457–2464.
- [19] H. Kato, K. Asakura, A. Kudo, *J. Am. Chem. Soc.* 125 (2003) 3082–3089.
- [20] W.J. Youngblood, S.H.A. Lee, K. Maeda, T.E. Mallouk, *Acc. Chem. Res.* 42 (2009) 1966–1973.
- [21] T. Inoue, A. Fujishima, S. Konishi, K. Honda, *Nature* 277 (1979) 637–638.
- [22] F. Solymosi, I. Tombácz, *Catal. Lett.* 27 (1994) 61–65.
- [23] M. Anpo, H. Yamashita, Y. Ichihashi, Y. Fujii, M. Honda, *J. Phys. Chem. B* 101 (1997) 2632–2636.
- [24] I.H. Tseng, J.C.S. Wu, H.Y. Chou, *J. Catal.* 221 (2004) 432–440.
- [25] Q.H. Zhang, W.D. Han, Y.J. Hong, J.G. Yu, *Catal. Today* 148 (2009) 335–340.
- [26] K. Koci, K. Mateju, L. Obalova, S. Krejčíková, Z. Lancy, D. Placha, L. Capek, A. Hospodkova, O. Solcova, *Appl. Catal., B* 96 (2010) 239–244.
- [27] T. Yui, A. Kan, C. Saitoh, K. Koike, T. Ibusuki, O. Ishitani, *ACS Appl. Mater. Interfaces* 3 (2011) 2594–2600.
- [28] K. Sayama, H. Arakawa, *J. Phys. Chem.* 97 (1993) 531–533.
- [29] Y. Matsumoto, M. Obata, J. Hombo, *J. Phys. Chem.* 98 (1994) 2950–2951.
- [30] P.W. Pang, Y.W. Chen, *Catal. Commun.* 8 (2007) 1546–1549.
- [31] Q. Liu, Y. Zhou, J. Kou, X. Chen, Z. Tian, J. Gao, S. Yang, Z. Zou, *J. Am. Chem. Soc.* 132 (2010) 14385–14387.
- [32] S.C. Yan, S.X. Ouyang, J. Gao, M. Yang, J.Y. Feng, X.X. Fan, L.J. Wan, Z.S. Li, J. Ye, Y. Zhou, Z.G. Zou, *Angew. Chem. Int. Ed.* 49 (2010) 6400–6404.
- [33] Y. Zhou, Z. Tian, Z. Zhao, Q. Liu, J. Kou, X. Chen, J. Gao, S. Yan, Z. Zou, *ACS Appl. Mater. Interfaces* 3 (2011) 3594–3601.
- [34] K. Iizuka, T. Wato, Y. Miseki, K. Saito, K. Kudo, *J. Am. Chem. Soc.* 133 (2011) 20863–20868.
- [35] E. Bae, N. Murakami, T. Ohno, *J. Mol. Catal. A: Chem.* 300 (2009) 72–79.
- [36] N. Murakami, Y. Kurihara, T. Tsubota, T. Ohno, *J. Phys. Chem. C* 113 (2009) 3062–3069.
- [37] E. Bae, N. Murakami, M. Nakamura, T. Ohno, *Appl. Catal., A* 380 (2010) 48–54.
- [38] L. Zhang, V.M. Menendez-Flores, N. Murakami, T. Ohno, *Appl. Surf. Sci.* 258 (2012) 5803–5809.
- [39] N. Murakami, S. Kawakami, T. Tsubota, T. Ohno, *J. Mol. Catal. A: Chem.* 358 (2012) 106–111.
- [40] V.M. Menendez-Flores, M. Nakamura, T. Kida, Z. Jin, N. Murakami, T. Ohno, *Appl. Catal., A* 406 (2011) 119–123.
- [41] N. Murakami, A. Ono, M. Nakamura, T. Tsubota, T. Ohno, *Appl. Catal., B* 97 (2010) 115–119.
- [42] E. Bae, T. Ohno, *Appl. Catal., B* 91 (2009) 634–639.
- [43] N. Murakami, T. Kamai, T. Tsubota, T. Ohno, *Catal. Commun.* 10 (2009) 963–966.
- [44] H. Kominami, M. Kohno, Y. Kera, *J. Mater. Chem.* 10 (2000) 1151.
- [45] H. Kominami, J. Kato, S. Murakami, Y. Ishii, M. Kohno, K. Yabutani, T. Yamamoto, Y. Kera, M. Inoue, T. Inui, B. Ohtani, *Catal. Today* 84 (2003) 181.
- [46] H. Kominami, Y. Ishii, M. Kohno, S. Konishi, Y. Kera, B. Ohtani, *Catal. Lett.* 91 (2003) 41.
- [47] A. Pottier, C. Chaneac, E. Tronc, L. Mazerolles, J.P. Jolivet, *J. Mater. Chem.* 11 (2001) 1116.
- [48] K. Tomita, V. Petrykin, M. Kobayashi, M. Shiro, M. Yoshimura, M. Kakihana, *Angew. Chem. Int. Ed.* 45 (2006) 2378.
- [49] M. Kakihana, K. Tomita, V. Petrykin, M. Yoshimura, M. Kakihana, *J. Mater. Sci.* 43 (2008) 2158.
- [50] R. Buonsanti, V. Grillo, E. Carlino, C. Giannini, T. Kipp, R. Cingolani, P.D. Cozzoli, *J. Am. Chem. Soc.* 130 (2008) 11223.
- [51] Q. Deng, M. Wei, X. Ding, L. Jiang, B. Ye, K. Wei, *Chem. Commun.* (2008) 3657.
- [52] T.A. Kandiel, A. Feldhoff, L. Robben, R. Dillert, D.W. Bahnemann, *Chem. Mater.* 22 (2010) 2050–2060.
- [53] Q.H. Zhang, W.D. Han, Y.J. Hong, J.G. Yu, *Catal. Today* 148 (2009) 335–340.
- [54] M. Kobayashi, K. Tomita, V. Petrykin, S. Yin, T. Sato, M. Yoshimura, M. Kakihana, *Solid State Phenom.* 124–126 (2007) 723–726.
- [55] H. Zhang, J.F. Banfield, *J. Phys. Chem. B* 104 (2000) 3481–3487.
- [56] M. Kobayashi, V. Petrykin, M. Kakihana, K. Tomita, *J. Am. Ceram. Soc.* 92 (S1) (2009) S21–S26.
- [57] T. Ohno, K. Sarukawa, M. Matsumura, *New J. Chem.* 26 (2002) 1167–1170.
- [58] X. Yang, T. Xiao, P.P. Edwards, *Int. J. Hydrogen Energy* 36 (2011) 6546–6552.
- [59] Y. Tian, T. Tatsuma, *J. Am. Chem. Soc.* 127 (2005) 7632–7637.
- [60] K. Naoi, Y. Ohko, T. Tatsuma, *J. Am. Chem. Soc.* 126 (2004) 3664–3668.
- [61] A. Zielinska, E. Kowalska, J.W. Sobczak, W. Liskowski, B. Ohtani, A. Zaleska, *Appl. Catal., B* 101 (2011) 504–514.
- [62] S. Link, El. M.A. Sayed, *J. Phys. Chem. B* 103 (1999) 4212–4217.
- [63] R. Jin, Y. Cao, C.A. Mirkin, K.L. Kelly, G.C. Schatz, J.G. Zheng, *Science* 294 (2001) 1901–1903.
- [64] J.J. Mock, M. Barbic, D.R. Smith, D.A. Schultz, S. Schultz, *J. Chem. Phys.* 116 (2002) 6755–6759.